materials

MDPI

Article

Soldering Characteristics and Mechanical Properties of Sn-1.0Ag-0.5Cu Solder with Minor Aluminum Addition

Yee Mei Leong and A.S.M.A. Haseeb *

Centre for Advanced Materials, Department of Mechanical Engineering, Faculty of Engineering, University of Malaya, Kuala Lumpur 50603, Malaysia; leongyeemei@siswa.um.edu.my
* Correspondence: haseeb@um.edu.my; Tel.: +60-3-79674492

Academic Editor: Geminiano Mancusi
Received: 26 May 2016; Accepted: 16 June 2016; Published: 28 June 2016

Abstract: Driven by the trends towards miniaturization in lead free electronic products, researchers are putting immense efforts to improve the properties and reliabilities of Sn based solders. Recently, much interest has been shown on low silver (Ag) content solder SAC105 (Sn-1.0Ag-0.5Cu) because of economic reasons and improvement of impact resistance as compared to SAC305 (Sn-3.0Ag-0.5Cu. The present work investigates the effect of minor aluminum (Al) addition (0.1–0.5 wt.%) to SAC105 on the interfacial structure between solder and copper substrate during reflow. The addition of minor Al promoted formation of small, equiaxed Cu-Al particle, which are identified as Cu_3Al_2. Cu_3Al_2 resided at the near surface/edges of the solder and exhibited higher hardness and modulus. Results show that the minor addition of Al does not alter the morphology of the interfacial intermetallic compounds, but they substantially suppress the growth of the interfacial Cu_6Sn_5 intermetallic compound (IMC) after reflow. During isothermal aging, minor alloying Al has reduced the thickness of interfacial Cu_6Sn_5 IMC but has no significant effect on the thickness of Cu_3Sn. It is suggested that of atoms of Al exert their influence by hindering the flow of reacting species at the interface.

Keywords: intermetallic; mechanical properties; nanoindentation; interfacial reaction; microstructure; differential scanning calorimetry; scanning electron microscopy; minor Al addition

1. Introduction

Restriction on the use of lead based solder in the electronic industry has led to extensive developments in lead free solders. Driven by the necessity to improve the reliability of lead free electronic products and by the trend towards miniaturization, researchers are putting intense efforts into improving the properties of Sn based solders. Sn-Ag-Cu (SAC solder) alloys have been a favored replacement for Sn-Pb solders. However, the currently used ternary eutectic (T_m = 217 °C) or near eutectic SAC solders have some drawbacks. These SAC solders were reported to have relatively high amount of undercooling (10–30 °C), as β-Sn requires large undercooling to nucleate and solidify. This large undercooling promotes the formation of large, plate-like Ag_3Sn structures that have been reported to cause joint embrittlement and reliability problem [1]. Research has been done on solders with lower silver content of, e.g., Sn-1.0Ag-0.5Cu (SAC105), in an attempt to inhibit the formation of Ag_3Sn and also to reduce the solder cost, as the price of Ag has increased dramatically in recent years [2–5]. Although it has been reported that SAC105 performs better in drop tests, it has a higher liquidus temperature, which requires a higher reflow profile than the eutectic Sn-3.8Ag-0.7Cu (SAC387) alloy [5]. It also performs poorly in thermal cycling tests [6]. These drawbacks have prompted researchers to modify the solder content by adding small amounts of other alloying elements to further improve its reliability and lower its melting temperature.

Fourth minor alloying elements (0.05–0.1 wt.%) that have been added into SAC solder include Ni, Co, Fe, Mn, Zn, Ti, Ce, In and Al [7–10]. The effects of the fourth alloying element on the microstructure and mechanical properties have been investigated. Improvements in mechanical properties such as shear strength [10], tensile strength [7], impact resistance [5], and creep resistance [7] have been reported. It has been observed that the addition of fourth alloying elements imparts their influence on the mechanical properties by modifying the microstructure of the solder. It was observed that the fourth alloying element modify the microstructure, by: (i) refining the microstructure of the solder matrix; (ii) suppressing brittle intermetallic compound (IMC) formation; and (iii) changing the morphology of the IMC in solder matrix/interface [11].

The addition of aluminum has attracted much interest in recent years. Research on Al addition as nanoparticles or minor alloying element has been reported [12–18]. Amagai [12] observed that the addition of 0.05% Al nanoparticles did not have any significant effect on the interfacial IMC. As for the addition of aluminum as minor alloying element, a few works on the effect of Al on the mechanical properties, microstructure and solder/Cu substrate interfacial reaction have been reported [2,9,11,14–18]. Previous studies have shown that minor addition of Al gives promising results in suppressing undercooling of β-Sn and reduced formation of brittle phase Ag_3Sn in SAC solder matrix [14]. It was found that Al addition (0.05 wt.%) results in excellent shear strength retention after thermal aging at 150 °C for up to 1000 h. Faizul et al. have investigated the effect of Al (0.1–2 wt.%) on the tensile strength of SAC105 [12,19]. They found that with 0.1 wt.% Al addition, Al reduced the yield strength and ultimate tensile strength (UTS) and promoted ductile fracture. When Al addition was more than 0.1 wt.%, the yield strength and ultimate tensile strength of the solder increased as a function of Al content and brittle fracture modes were seen.

A couple of studies dealt with the effects of Al on the bulk microstructure and interfacial IMC between solder and copper substrate [15,16,18]. With the addition of Al into Sn-Ag (SA) solder, Al_2Cu IMC and ambiguous Al-Cu IMC were found in the bulk microstructure of SA solder on copper substrate after reflow [16,18]. On the other hand, only ambiguous Al-Cu IMC (Anderson et al. reported it as δ-$Cu_{33}Al_{17}$) was found in the bulk microstructure of SAC [14,19]. Though the reported effect of Al on the bulk microstructure seen by other researchers seems consistent, there are contradictory reports on the effects of Al addition on the interfacial solder/Cu reaction. With addition of 0.5 wt.% of Al into SA solder, Xia et al. observed a spalled layer of Al_2Cu compound layer near the interface and the suppression of the growth of the Cu_6Sn_5 layer. When Al was added up to 1 wt.%, a layer of Al_2Cu compound was formed at the solder/Cu interface, which completely replaced Cu_6Sn_5 layer [15]. On the other hand, Kotadia et al. reported that spherical Al-Cu IMC spalled away from the solder matrix when Al was depleted in the solder and there was no suppression of the growth of interfacial Cu_6Sn_5 layer when 0.5 to 2.0 wt.% of Al was added in to SA solder [18]. Li et al. have reported that with the addition of 1 wt.% Al into SAC387 solder, layered δ-Al_2Cu_3 formed at the interface after 10 min reflow and the growth of the Cu_6Sn_5 layer was reduced [16]. Dhaffer et al. have investigated the effect of 0.1.wt.% Al addition on the interfacial reaction by dipping method, they reported that 0.1% Al addition have suppressed the growth of Cu_6Sn_5 layer [20]. Until now, no detailed study has been done for the effect of minor Al addition (<1 wt.%) on interfacial reaction of SAC/Cu.

Nanoindentation as a mechanical testing method has attracted a great deal of attraction in many fields of research as it has the ability to measure the properties of sample in extremely small scales such as thin films and coating in nanometer range [21]. This technique is well suited to investigate the mechanical properties of IMCs, which have thicknesses of only several nanometers/micrometers. Cu-Al IMC was reported to form in SAC even with addition of as low as 0.05 wt.% [22]. Besides, it has been reported that Al is likely to substitute into Cu_6Sn_5 as well [14] Previous studies with addition such as Ni, and Mn have shown that solubility of minor alloying element in Cu_6Sn_5 could alter the nanomechanical properties of Cu_6Sn_5 [14]. Thus, understanding the mechanical properties of Cu-Al IMC and Cu_6Sn_5 is essential in the understanding of deformation behavior and failure mechanisms in lead-free solder joints.

The present work investigates the effect of Al on the interfacial IMC between SAC105 solder alloy and copper substrate. This work concentrates on the effect of the lower percentage of Al (0.1–0.5 wt.%)

on the Cu–Sn reaction during reflow and isothermal aging. As has been noted earlier [15,16], absence of Cu in the solder led to the formation of Al_2Cu and Al-Cu IMC near/at the interface during reflow, and the IMCs tended to spall away from the solder matrix when Al was depleted in solder, thus complicating the situation at the interface. With the presence of Cu in SAC solder, it is expected that Al will react with Cu in the bulk and thus provide a more simplified scenario at the interface, which may lead to a better understanding of the effects of Al. This study concentrates on the lower percentage of Al (0.1%–0.5%), as higher percentages may lead to formation of Al_2Cu and other IMCs at the interface. Furthermore, this study investigates the nanomechanical properties of Cu-Al IMC particles and also examines whether addition of Al would affect the nanomechanical properties of Cu_6Sn_5.

2. Results

2.1. Differential Scanning Calorimetry

Figure 1 shows the Differential Scanning Calorimetry (DSC) curves for SAC105, SAC105 + 0.1Al, SAC105 + 0.3Al and SAC105 + 0.5Al. During heating, SAC105 and SAC105 + 0.1Al solder show an onset melting temperature (T_m) of 216.84 °C ± 0.50 and 216.43 °C ± 0.38, respectively. This onset temperature corresponds to the ternary eutectic reaction (T_m = 217 °C) of Sn-Ag-Cu alloy, L → Ag_3Sn + Cu_6Sn_5 + Sn [23]. Two prominent peaks were seen at ~221 °C and ~228 °C in SAC105 and SAC105 + 0.1Al (Figure 1a,b). These two peaks were associated with the eutectic temperature for Sn-Ag (L → Ag_3Sn + Sn) and Sn-Cu (L → Cu_6Sn_5 + Sn), respectively. As the amount of Al was added up to 0.3 wt.%, there is a change in the DSC curve (Figure 1c). The onset temperature was shifted to 221.14 °C ± 0.36 and 221.65 °C ± 1.02, respectively for SAC105 + 0.3Al and SAC105 + 0.5Al which corresponded to Sn-Ag eutectic temperature (T_m = 221 °C). For SAC105 + 0.3Al, a first small peak of heat absorption appears at 224 °C, followed by a second larger peak of heat absorption at ~231 °C (Figure 1c). For SAC105 + 0.5Al, only a large peak of heat absorption appears at ~231 °C (Figure 1d). The peak at ~231 °C corresponds to the melting temperature of Sn (T_m = 231 °C).

During cooling, the nucleation temperature was determined by the onset solidification of the exothermic peak (Figure 1b). SAC105 has an onset solidification at 200.12 ± 0.64 °C. Addition of aluminum to SAC105 shifted the exothermic peak to the right, where the onset solidification temperature is 215.84 °C ± 1.39, 217.74 °C ± 0.83 and 219.17 °C ± 0.21 for SAC105 + 0.1Al, SAC105 + 0.3Al and SAC105 + 0.5Al, respectively.

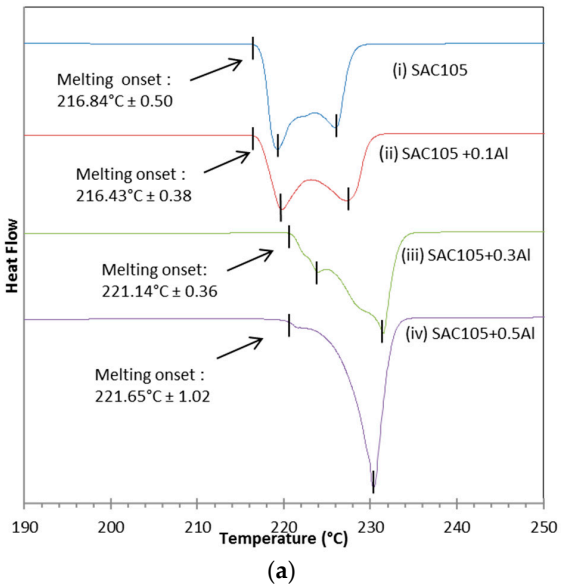

(**a**)

Figure 1. *Cont.*

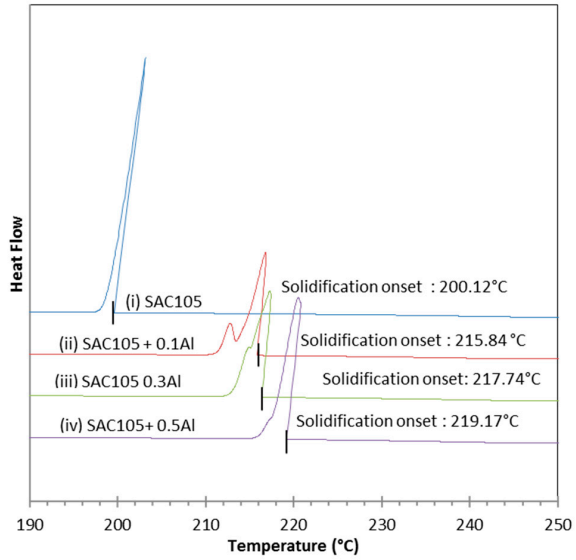

(**b**)

Figure 1. DSC curves for as cast SAC105, SAC105 + 0.1Al, SAC105 + 0.3Al and SAC105 + 0.5Al alloys: (**a**) heating; and (**b**) cooling.

The degree of undercooling, ΔT, was defined by the difference of two onset temperatures in cooling and heating curve. In Table 1, it can be seen that SAC105 has the largest undercooling of ~17 °C. The addition of Al into SAC105 solder reduced the degree of undercooling significantly in all cases where Al was added.

Table 1. Onset of melting, onset of solidification and undercooling of SAC105, SAC105 + 0.1Al, SAC105 + 0.3Al and SAC105 + 0.5Al.

Solder	Onset of Melting (°C)	Onset of Solidification (°C)	Undercooling (°C)
SAC105	216.84 ± 0.50	200.12 ± 0.64	~17
SAC105 + 0.1Al	216.43 ± 0.38	215.84 ± 1.39	~0.6
SAC105 + 0.3Al	221.14 ± 0.36	217.74 ± 0.83	~3.4
SAC105 + 0.5Al	221.65 ± 1.02	219.17 ± 0.21	~2.48

2.2. Microstructure

Figure 2a–h shows the cross sectional Scanning Electron Microscopy (SEM) images of as-received solder alloys and reflowed solder joints prepared on copper substrates. Cross sectional images of as-received SAC105 samples show primary Sn phase having a lighter contrast while the darker contrast phase represents Cu_6Sn_5. The Cu_6Sn_5 formed a continuous network in the as-cast SAC105 solder and fine Ag_3Sn particles are also seen in the as-cast solder. With the addition of 0.1 wt.% Al, Cu_6Sn_5 phase and particles of another new darker phase are seen distributed in the lighter contrast Sn phase. The darker particles are seen to agglomerate in the Sn phase (Figure 2b). With the addition of 0.3 wt.% and 0.5 wt.% Al, elongated shapes of new darker IMC phase are seen distributed in the lighter contrast Sn phase. It can be seen that the Sn grain size decreases with Al addition in the as-received alloys. After reflow, the bulk microstructure of the reflowed solder was different from that of the as-received solder. From Figure 2e,f it can be seen that Cu_6Sn_5 and Ag_3Sn particles are larger after 1 × reflow as compared to Figure 2a,b. After 1 × reflow, with the addition of 0.3 wt.% and 0.5 wt.% Al, equiaxed darker IMC was seen distributed in Sn phase instead of elongated shape of new darker IMC in the as-received sample. Sn grain size reduction as a function of Al content still persists in reflowed sample.

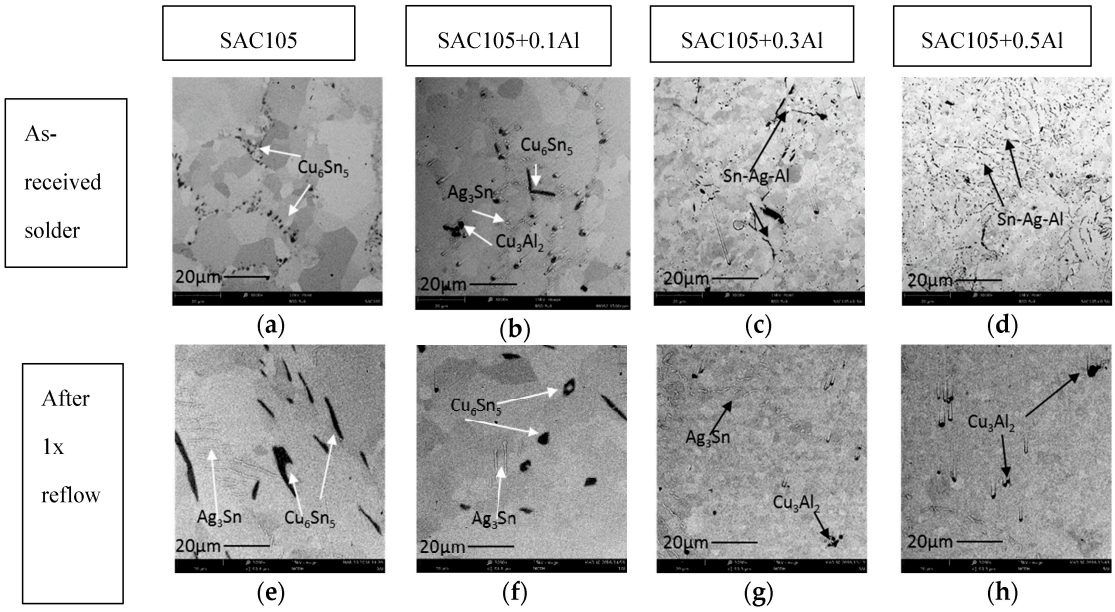

Figure 2. SEM images of cross sectional samples of bulk microstructure of as cast (**a**–**d**) and after 1 × reflow (**e**–**h**) of SAC105, SAC105 + 0.1Al, SAC105 + 0.3Al and SAC105 + 0.5Al.

Figure 3a shows the optical microscope cross-sectional images of SAC105 + 0.5Al near top surface of solder after 1 × reflow. It can be seen that the new darker phase equiaxed IMC agglomerated and was mostly found near the top surface of the solder joint. Agglomeration of the new darker phase near the top surface of solder is also found SAC105 + 0.3Al. Figure 3b shows the new darker phase equiaxed IMC under high magnification. It can be seen that the new faceted IMC particles have varied sizes, ranging from 1 to 5 μm.

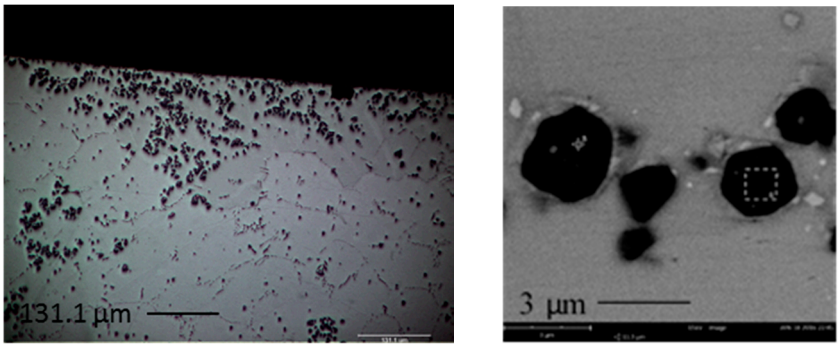

Figure 3. (**a**) Optical microscope cross sectional images SAC105 + 0.5Al near top surface of the solder after 1 × reflow and (**b**) FESEM images of equiaxed but faceted IMCs found at cross-sectioned of SAC105 + 0.5Al.

Energy-dispersive X-ray Spectroscopic (EDS) analysis was conducted on the new IMC phase found in SAC105 + 0.1Al, SAC105 + 0.3Al and SAC105 + 0.5Al. Analysis results indicated that the composition of the new phase was 60–65 at.% Cu, 35–40 at.% Al. EDS Line scan and elemental mapping analysis were also conducted on the new IMC phase (Figures 4 and 5). Both analysis confirmed that this darker IMC phase consists of only Al and Cu. Based on the ratio of Al and Cu content, possible identification of this darker IMC phase is Cu_3Al_2 (δ) or Cu_9Al_4 (γ_1), both of which could exist in the temperature range below 300 °C [24].

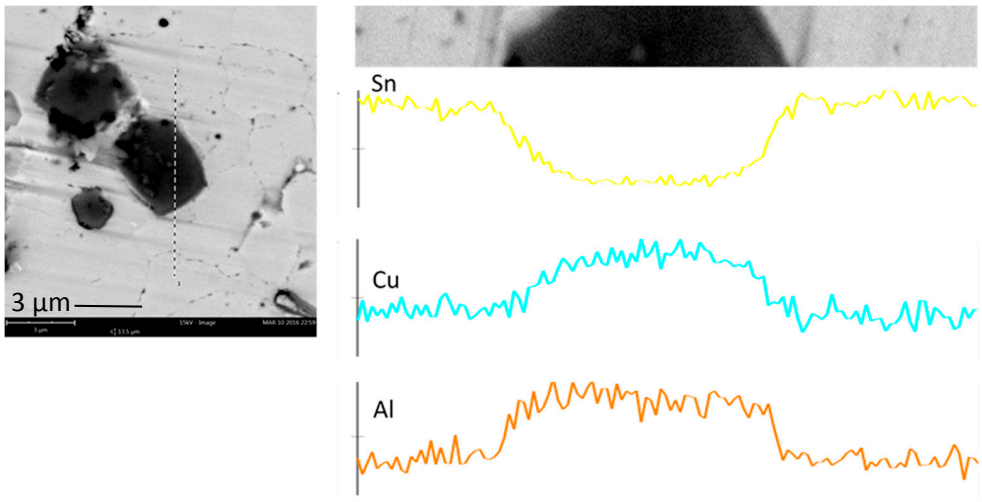

Figure 4. EDS line scan across equiaxed IMCs in SAC105 + 0.5Al.

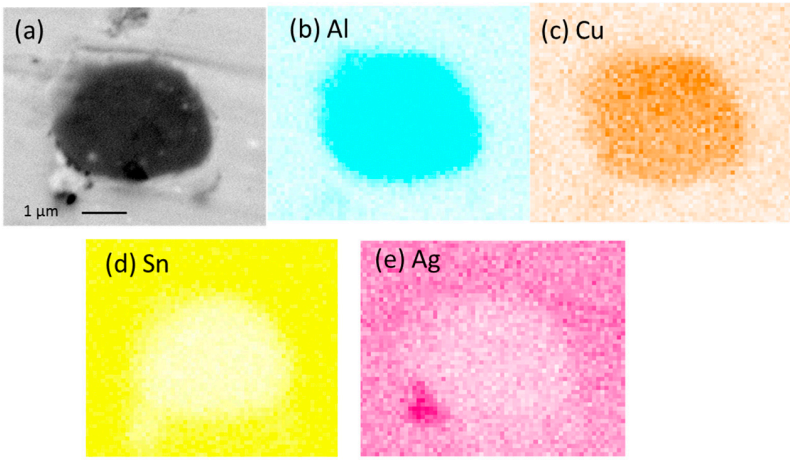

Figure 5. (**a**) Cross-sectioned image of SAC105 + 0.5Al after 1 × reflow. Elemental maps for the constituent elements: (**b**) Al; (**c**) Cu; (**d**) Sn; and (**e**) Ag.

In the previous studies on minor addition of Al, many researchers attempted to identify Cu-Al IMC by EDS analysis. There are a few Cu-Al binary phases that have compositions close to each other, such as γ_1-Cu_9Al_4, ζ_2-Cu_4Al_3, and δ-Cu_3Al_2. This makes it difficult for researchers to accurately identify the exact Cu-Al phase form [2,17,20]. Similarly, in this study, EDX analysis could not provide clear identification for the Cu-Al compound. Anderson et al. who studied the effect of Al addition on the microstructure of solder have identified the Cu-Al IMC as δ-$Cu_{33}Al_{17}$. They did so by casting out a Cu-Al block which has the similar composition with the Cu-Al IMC they obtained in the bulk solder, and analyzed it using X-ray diffraction (XRD) [14]. Though Anderson et al. have chosen to refer to it as δ-$Cu_{33}Al_{17}$, the general nomenclature for these IMC is also known as δ-Cu_3Al_2 [24]. By comparing the morphology of Cu-Al IMC (Figure 3a) in this study to δ-$Cu_{33}Al_{17}$ [14], it can be seen that they both exhibit a similar morphology (equiaxed and faceted dark color appearance under Field-emission scanning electron microscopy (FESEM) and size (size varied from 1 to 5 µm)). Thus, it would be logical to assume both IMC are of the same kind, and it will be referred to as Cu_3Al_2 in the following discussion.

2.3. Interfacial Reaction after Reflow

Figure 6 shows cross-sectional FESEM micrographs at the solder/Cu interface after 1 × reflow. A typical scallop type Cu_6Sn_5 layer forms at the SAC105/Cu interface after reflow (Figure 6a). Upon the addition of aluminum, the scallop morphology is still seen, but the IMC becomes more flat as Al is

added up to 0.5 wt.% (Figure 6c). The IMC height is reduced with the addition of Al. The average thickness of the total IMC layer is plotted as a function of Al content in Figure 7. The influence of Al addition on the interfacial IMC thickness is obvious. The thickness of the interfacial IMC does not seem to vary with the Al content of the solder in the range 0.1–0.5 wt.%. This may indicate that the addition of Al beyond a certain percentage does not bring additional benefit in terms of suppression of IMC growth. Cu_6Sn_5 was the only IMC found at the interface, and no trace of Al in Cu_6Sn_5 and Al-Cu compound could be detected at the interface of all aluminum-added solder.

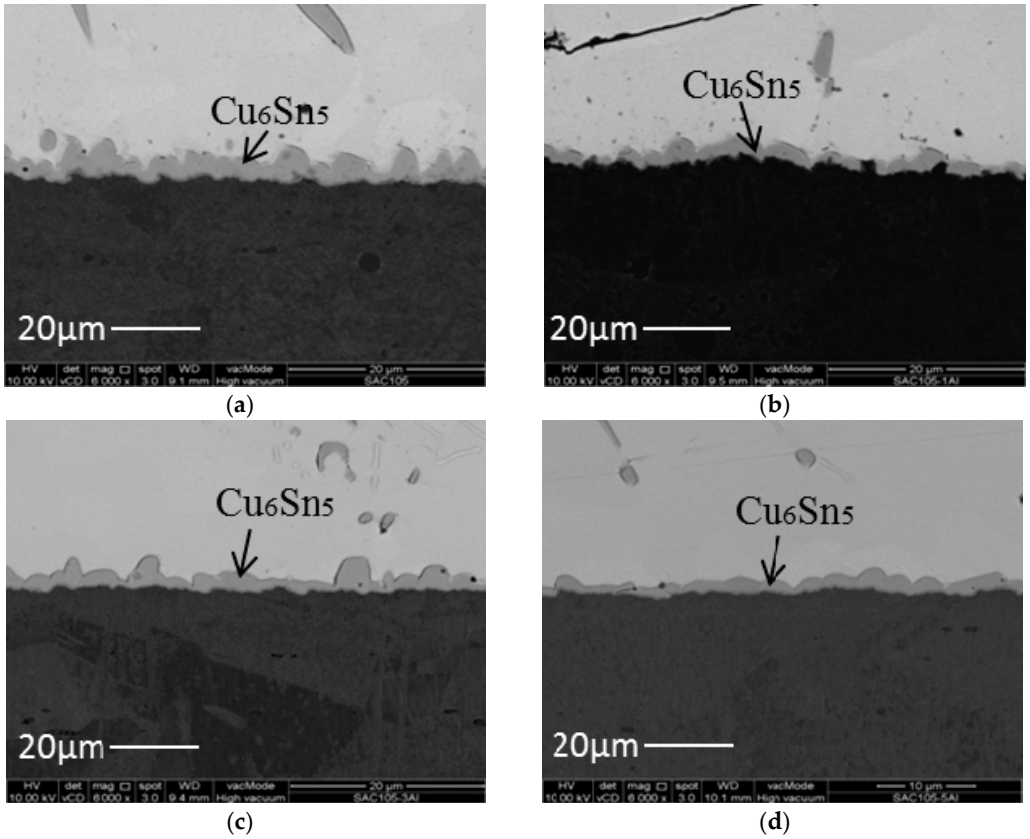

Figure 6. Cross sectional FESEM micrographs of: (**a**) SAC105; (**b**) SAC105 + 0.1Al; (**c**) SAC105 + 0.3Al; and (**d**) SAC105 + 0.5Al after 1 × reflow.

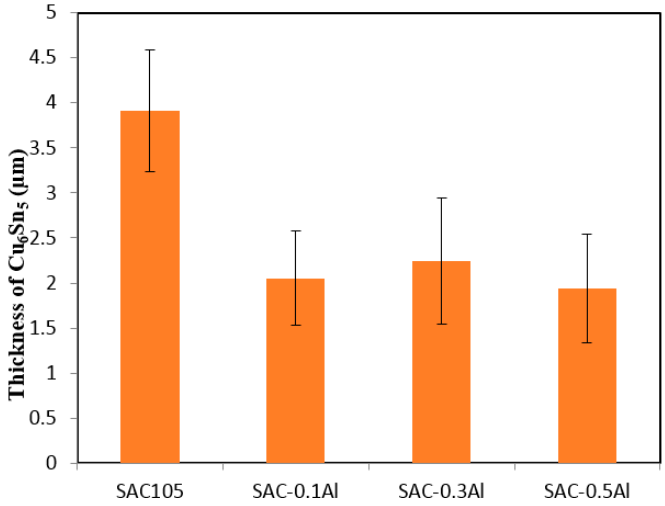

Figure 7. Variation of Cu_6Sn_5 thickness with Al content during 1 × reflow.

2.4. Top View of Cu_6Sn_5 Solder after 1 × Reflow

Figure 8a shows top view image of deeply etched SAC105 + 0.5Al after 1 × reflow. Prior to FESEM imaging, both samples were deeply etched in a mixture of 93% CH_3OH, 5% HNO_3 and 2% HCl to remove the solder matrix and thereby expose the interfacial IMC. The IMC grains found on the interface of SAC105 and SAC105 + 0.5Al were identified as Cu_6Sn_5. It can be seen from the images that SAC105 + 0.5Al shows somewhat faceted Cu_6Sn_5 grains. Under high magnification in the high Al concentration region, small and agglomerated particles are seen (encircled in yellow dotted line). EDS analysis was done on the high Al concentration particle. Figure 8b–d shows the EDS elemental maps. Under high resolution imaging and elemental mapping, Al, Ag and Cu were detected on the surface of the exposed IMC. In Figure 8b, the presence of Al is indicated in green. The region of high concentration of Al is encircled in yellow. It can be seen that the region with high Al concentration corresponds to that of Cu (compare Figure 8b,c). The agglomerated particles are identical to the Cu-Al IMC that was found in the bulk microstructure. The elongated and plate-like particles (right corner of Figure 8d) on the Cu_6Sn_5 IMC grains are identified as Ag_3Sn.

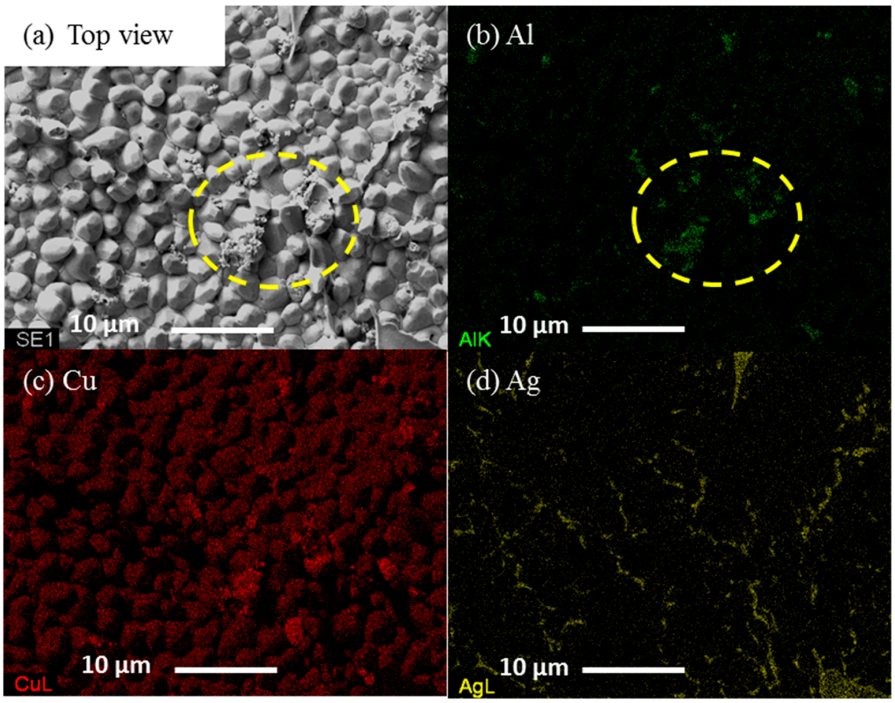

Figure 8. (**a**) Top view image of deeply etched SAC105 + 0.5Al after 1 × reflow. Elemental maps for the constituent elements: (**b**) Al; (**c**) Cu; and (**d**) Ag.

2.5. Interfacial Reaction After Isothermal Aging

After 1 × reflow, some of the solder samples were also subjected to isothermal aging at 150 °C for up to 720 h in order to study the effects of Al addition on the solid state reaction between solder and copper substrate. Figure 9 shows the cross sectional images of isothermally aged SAC105, SAC105 + 0.1Al, SAC105 + 0.3Al and SAC105 + 0.5Al. After thermal aging for 720 h, another intermetallic layer (darker layer) formed in between the first intermetallic layer and Cu substrate in both SAC and SAC + Al solders. EDS was used to determine the composition of each layer. It is confirmed by elemental ratio by EDS analysis that the outer layer is Cu_6Sn_5 and the inner layer is Cu_3Sn. Within the resolution of EDS, there was no aluminum detected in both Cu_6Sn_5 and Cu_3Sn after thermal aging. The morphology of Cu_6Sn_5 and Cu_3Sn are seen to be similar in SAC105 and SAC105 + Al solders.

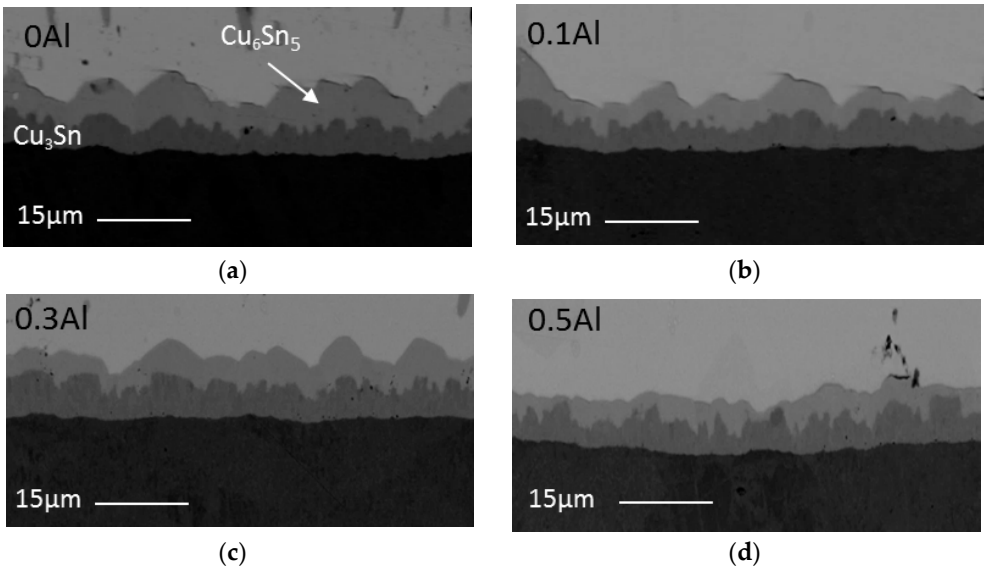

Figure 9. Cross sectional images of: (**a**) SAC105; (**b**) SAC105 + 0.1Al; (**c**) SAC105 + 0.3Al; and (**d**) SAC105 + 0.5Al after aging at 150 °C for 720 h.

From Figure 9, it is seen that the addition of Al up to 0.5 wt.% has slowed down the growth of the total interfacial IMCs. Figure 10 shows the thickness of Cu_6Sn_5 and Cu_3Sn plotted as a function of Al content. It can be seen that Cu_6Sn_5 is reduced as Al is added, up to 0.5 wt.%. However, the thickness of Cu_3Sn is almost the same for all samples.

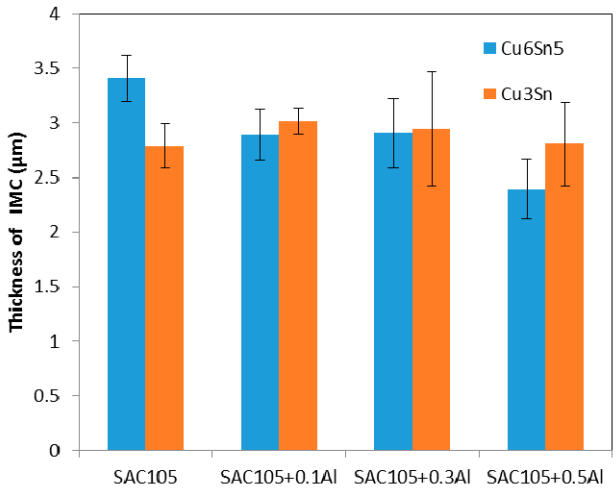

Figure 10. Variation of thickness of IMC with Al content after aging at 150 °C for 720 h.

2.6. Mechanical Properties

Indentation testing was carried out on bulk solder and the intermetallic phase in the solders, e.g., Cu_6Sn_5 and Cu_3Al_2. The hardness of the bulk solder was determined by Vickers hardness test while the hardness of individual intermetallic phase was determined by nanoindentation. Figure 11 shows the hardness of solder with varying Al content. It can be seen that the hardness of the solder increases as a function of Al content. SAC105 exhibited hardness of 9.78 HV while SAC105 + 0.5Al exhibited the highest hardness value of 14.12 HV. The result of SAC105 is in good agreement with other studies [25,26].

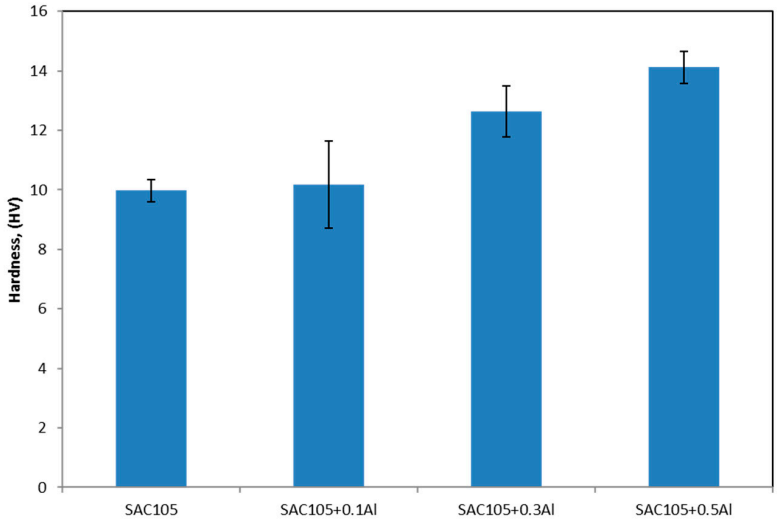

Figure 11. Variation of Vickers hardness with Al content for as received samples.

Figure 12 shows typical load displacement data obtained through indentations performed on Sn, Cu_6Sn_5 and Cu_3Al_2 of a maximum load of 500 μN. For a test of the same maximum load, the maximum penetration of the indenter for Sn-Ag-Cu solder is approximately 4.5 times of that measured for Cu_6Sn_5 and Al_3Cu_2. The solder matrix, as expected, is very soft, with a hardness of 0.23–0.3 GPa. The matrix exhibited significant plasticity. Upon unloading, the solder recovers only approximately 10 nm of the 230 nm that the indenter penetrated. In contrast to the solder, both intermetallics are significantly harder: Cu_6Sn_5 (~6.2 GPa) and Al_3Cu_2 (~10.50 GPa). The intermetallics typically recover around 40% of the maximum penetration of the indenter upon unloading. From this, the deformation of the intermetallic phases was found to be both elastic and plastic, while the deformation of the solder is found to be primarily plastic [26]. Scanning probe microscopy (SPM) was used to accurately perform indentation on specific IMC phases. It was also used to observe the residual indents, as shown in Figure 13. As expected from the nanoindentation data in Figure 12, the residual indents in the solder were much larger than in intermetallics (Figure 13). All of the residual indents observed for the intermetallics exhibited a smooth profile with no detected pile-up or sink-in of material, while softer materials like Sn exhibit a pile-up behavior.

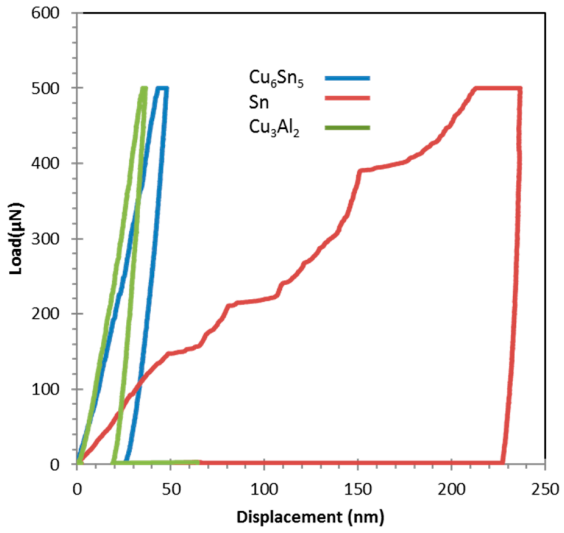

Figure 12. Load displacement data obtained for 500 μN maximum load indentations performed on Sn, Cu_6Sn_5 and Cu_3Sn.

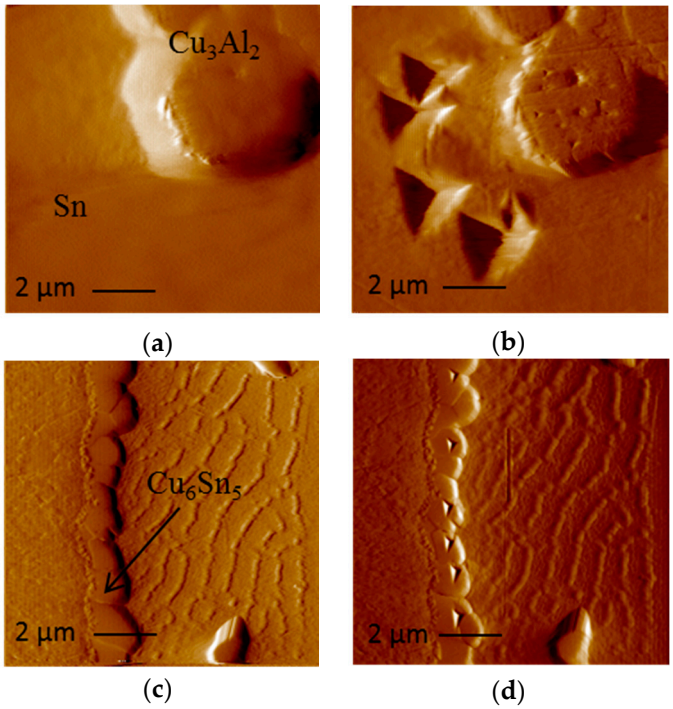

Figure 13. Scanning probe microscopy image of: (**a**) Sn and Cu_3Al_2 before indentation; (**b**) Sn and Cu_3Al_2 after indentation; (**c**) Cu_6Sn_5 before indentation; and (**d**) Cu_6Sn_5 after indentation of SAC105 + 0.1Al.

Hysitron nanoDMA with CMX correction and maximum load of 1000 μN was used to perform continuous nanoscale dynamic mechanical measurement of Cu_3Al_2. Hardness and elastic modulus of Cu_3Al_2 could be obtained as a function of indentation depth. Figure 14 shows the hardness and elastic modulus of Cu_3Al_2 plotted against indent displacement. The hardness and elastic modulus of Cu_3Al_2 was lower near the surface but was fairly constant at depths greater than ~15 nm. The results are similar to that obtained from quasi-static measurement with maximum load of 500 μN.

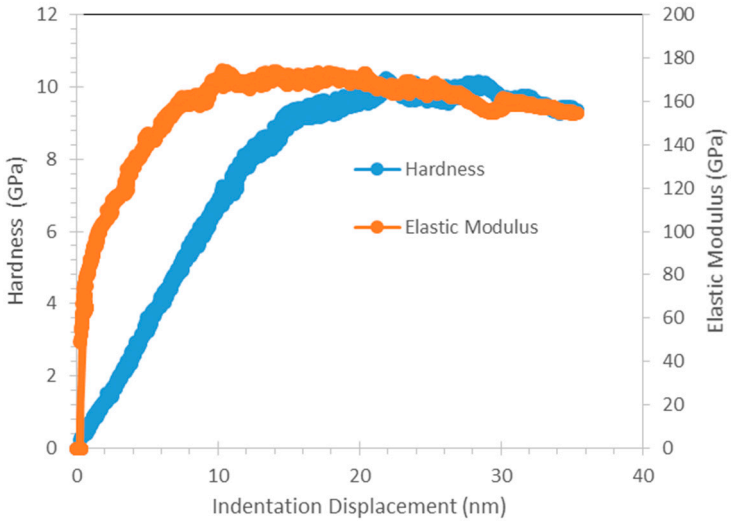

Figure 14. Hardness and Elastic Modulus of Cu_3Al_2 plotted against indent displacement.

As seen in Table 2, Sn has hardness and elastic modulus of 0.22–0.36 GPa and ~50 GPa, respectively, while Cu_6Sn_5 has hardness and elastic modulus of ~6.2 GPa and ~92–110 GPa, respectively. The results

are in good agreement with other studies [27–29]. On the other hand, Cu_3Al_2 exhibits a much higher hardness and elastic modulus as compared to Sn and Cu_6Sn_5, with a hardness of ~10.50 GPa and an elastic modulus of ~170.08 GPa.

Table 2. Hardness and modulus of Pure Sn, Cu_6Sn_5, and Cu_3Al_2.

Element/Compound	SAC105		SAC + 0.1Al	
	E (GPa)	H (GPa)	E (GPa)	H (GPa)
Sn	49.43 ± 7.93	0.29 ± 0.07	50.43 ± 4.86	0.23 ± 0.04
Cu_6Sn_5	92.25 ± 16.24	6.20 ± 0.59	100.99 ± 10.09	6.26 ± 1.07
Cu_3Al_2	–	–	170.08 ± 12.92	10.52 ± 1.71

3. Discussion

From the DSC curves (Figure 1), it is found that when 0.1 wt.% of Al was added to the solder, the endothermic curve remains similar to that of SAC105. Both SAC105 and SAC105 + 0.1Al exhibit twin peaks endothermic curve. The onset melting temperature of SAC105 + 0.1Al is the same as that of SAC105, which is ~217 °C. This corresponds to Sn-Ag-Cu ternary eutectic temperature. When the percentage of Al is increased to 0.3 wt.% and 0.5 wt.%, the onset of melting temperature shifts to ~221 °C (Sn-Ag eutectic temperature) [30]. The DSC curves of SAC105 + 0.3Al and SAC + 0.5Al solders are similar to the DSC curve of non-eutectic Sn-Ag solder [31]. This shows that free Cu atoms are not available in SAC105 + 0.3Al and SAC + 0.5Al solders as Sn-Ag-Cu solder alloy always shows the onset melting at ~217 °C [32]. One possible explanation for this is the formation of Cu_3Al_2 compound, which has reduced the available Cu in the bulk solder to react with Sn and Ag. The Cu_3Al_2 compound already formed in the as-received samples, which were supplied in the as-cast condition. As seen in Figure 2b–d, Cu_3Al_2 is formed in the as-cast solder. Cu_3Al_2 has a higher melting temperature of 960 °C [33]. Thus, during the melting of solders for up to 300 °C, the stable Cu_3Al_2 IMC did not react and this lowers the activity of Cu in solder melts. The lack of free Cu atom in the solder is further indicated by the shift of a prominent peak in the DSC curves of SAC105 and SAC105 + 0.1Al. The ~228 °C (Sn-Cu eutectic temperature) peak in SAC105 and SAC105 + 0.5Al has shifted to ~231 °C (T_m of Sn = 232 °C) in SAC105 + 0.3Al and SAC105 + 0.5Al. This shift indicates that the deficiency of Cu atom in SAC105 + 0.3Al and SAC105 + 0.5Al has reduced the strong eutectic reaction of Sn-Cu, $L \rightarrow Cu_6Sn_5$ + Sn. With Al addition, the peak indicating Sn melting is seen, as fractions of un-melted Sn remaining in the solder melted when temperature increased to 232 °C [30].

Table 1 shows that SAC105 has the largest undercooling of ~17 °C. This is well within range of undercooling values, 10–30 °C reported for Sn-Ag-Cu solder [1]. This is because β-Sn requires large undercooling to induce nucleation and solidification [1]. The presence of Al in SAC105 has reduced the undercooling significantly. It is seen that with addition of Al up to 0.5%, undercooling has reduced to 1–5 °C. Kotadia et al. and Anderson et al. have observed the effect of Al in reducing undercooling of Sn-3.5Ag and Sn-3.5Ag-0.95Cu solder to 7 °C and 4 °C respectively [14,34]. The addition of minor alloying element into solder has been one of the effective ways of reducing undercooling by promoting nucleation of β-Sn. Minor alloying atoms which have a much higher melting temperature can exist in molten Sn and provide heterogeneous site for β-Sn nucleation. In the case of Al as minor alloying, Cu_3Al_2 compound is formed even when the addition of Al is as low as 0.1%. During exothermic reaction in DSC, the existing Al-Cu intermetallic compounds act as a preferential site to promote heterogeneous nucleation of β-Sn, and thus lowering the undercooling of SAC105.

Segregated Cu_3Al_2 IMC was found near the top surface of the sample with addition of Al after 1 × reflow. One of the possible reasons could be that, during reflow, solders are melted on the Cu substrates at 250 °C, the Cu_3Al_2 particles are not wet by the molten solder, thus they are not drawn into the melt as the molten solder particles solidify. This causes rejection of the Cu_3Al_2, which remain near the surface/edges of the solder after reflow. Another possible reason for the segregation of

Cu_3Al_2 particles at the edge/surface could be attributed to the buoyancy effects. The density of Cu_3Al_2 particles is 6.278 g/cm^3, which is lower than the density of liquid Sn, 6.99 g/cm^3 [35]. Thus, during reflow, the less dense Cu_3Al_2 particles migrate to the surface/edges. Kotadia et al. have reported the segregation of Al_2Cu in SA solder. They suggested that the segregation of Al rich phase and Al-Cu compound is caused by Stokes and Marangoi motion, which is due to large stable liquid miscibility gap in binary Sn-Al and ternary Sn-Ag-Al [18].

Minor alloying elements which could affect the growth of Cu-Sn compound are divided into two categories: (i) elements that show marked solubility in either one or both of the Cu-Sn IMCs; and (ii) elements that do not significantly dissolve in either of the Cu–Sn IMCs [11]. The effect of elements in category 1 on IMC growth could be explained by using thermodynamic argument. These elements stabilize Cu_6Sn_5 and decrease the growth of Cu_3Sn. The elements in category 2 do not have a prominent effect on IMC as they only affect the growth of IMC layers indirectly. It can be seen from Figures 4 and 5 that the addition of Al has reduced the growth of Cu_6Sn_5. Though Anderson et al. have suggested Al has some solubility in Cu_6Sn_5, no trace of Al could be found in Cu_6Sn_5 in this study. In this study, the addition of up to 0.5 wt.% Al did not alter the scallop morphology of Cu_6Sn_5 [14]. Scallop type IMC formation is promoted by higher value of the IMC/liquid solder interfacial energy.

There is very limited amount of information available on the influence of Al on the Cu–Sn reaction. Li et al. have reported the suppression of Cu_6Sn_5 IMC growth with addition of 1% Al. They suggested that the suppression is due to the formation of an Al-Cu IMC layer at the interface, which acts as a barrier for Cu and Sn diffusion [16]. However, Al-Cu IMC layer is not found at the interface in this study as the amount of Al added is less ($\leqslant$5%). Dhaffer et al. have also reported suppression of Cu_6Sn_5 IMC growth with addition of 0.1% Al during dip soldering and solid state reaction [20]. The Cu_3Al_2 IMC found at the Cu_6Sn_5/Sn interface (Figure 8) could account for the suppression of Cu_6Sn_5. This is seen in previous work where Zn found at the Cu_6Sn_5/Sn interface, hindered the flow of copper atoms to the solder thereby slowing down the IMC growth [36]. Thus, the segregation of Al atoms at the IMC/Sn interface may have similar effect on the growth of IMC, by hindering the flow of Cu or Sn atom. With minor Al addition, most of the Al reacts with Cu in the bulk solder to form Cu_3Al_2. Hence, Al does not form a layer of compound at the interface. Reduction of free Cu atom in the bulk solder could also be attributed to the retardation of Cu_6Sn_5 growth. When the amount of Al in the solder increased ($\geqslant$0.5 wt.% Al in SA, $\geqslant$1 wt.% Al in SAC), it formed a layer of Cu-Al compound at the solder/Cu interface [15,16]. By their presence at the interface, Cu_3Al_2 IMC hinders the flow of Cu or Sn atom to the solder thereby retarding IMC growth during reflow.

During isothermal aging, the Cu_6Sn_5 IMC layer grows by interdiffusion of Cu and Sn and reaction with each other, while the Cu_3Sn IMC forms and grows by reactions between the Cu substrate and Cu_6Sn_5 IMC layer, as given in the equation below [11]:

$$Cu_6Sn_5 + 9Cu \rightarrow 5Cu_3Sn \quad (1)$$

The presence of Cu_3Al_2 IMC at the Cu_6Sn_5/Sn interface hinders the flow of Cu or Sn atom to the solder, however it does not affect the reaction in Equation (1). Cu_3Sn grows by consuming Cu_6Sn_5 that is formed during reflow. Thus, the thickness of Cu_3Sn was not significantly affected by the addition of Al in solder. On the other hand, with slower interdiffusion of Cu and Sn at the interface (due to presence of Cu_3Al_2) and Cu_3Sn formation by consumption of Cu_6Sn_5, the thickness of Cu_6Sn_5 was reduced in SAC105 + Al solder.

The addition of Al has increased the hardness of bulk solder. This could be due to the grain refinement of Sn, which can be seen in Figure 3. Kim et al. has also reported that addition of Al as low as 0.01 wt.% could refine the Sn grain of Sn-Cu solder [8]. From nanoindentation, Cu_3Al_2 that are found in all SAC + Al solder exhibits higher hardness than other elements in SAC105 + Al. This seems promising in strengthening the solder joints. However, its high elastic modulus should be considered as well, as high elastic modulus could be detrimental for impact testing. Thus, further testing need to be done to further verify the effects of strengthening effects of Cu_3Al_2.

In spite of the incorporation by only a small fraction, Al is clearly seen to have influenced decisively on the hardness, undercooling of solder and the interfacial characteristics during reflow. However, the amount of Al must be kept below 0.3 wt.% in order to avoid large Cu_3Al_2 agglomeration, which could affect the performance of solder.

4. Materials and Methods

SAC105-xAl (where x = 0, 0.1, 0.3, 0.5 wt.%) were fabricated by Beijing Compo Advanced Technology Co. Ltd. (Beijing, China). All the solder alloys were prepared in rod shape (0.7 cm diameter, 15 cm length). The solder alloy was then cut into thin disks with 1 mm thickness by using electric discharge machining (EDM, A500W, Sodick, Schaumburg, IL, USA).

As-received solder was prepared for micro-examination by standard metallographic technique which included, cutting, mounting, grinding (up to 3000 grit paper) and polishing (diamond paste with size 9 μm, 6 μm, 3 μm, 1 μm and colloidal silica with size 0.2 μm). The microstructure of the as-received SAC105-Al solders was characterized by Field emission scanning electron microscope (FESEM, FEI-FEG450, FEI, Houston, TX, USA) and intermetallic compound (IMC) composition was investigated by energy dispersive X-ray spectroscope (EDS, EDAX-Genesis Utilities, EDAX, Mahwah, NJ, USA). Differential scanning calorimeter, DSC (DSC Q20, TA Instruments, New Castle, DE, USA) was used to evaluate the effect of the addition of Al on the onset melting and onset solidification temperature of the SAC105 solder. Each of the samples was weighed to approximately 10 mg and placed on an aluminum pan and covered with a lid. It was then heated from 25 °C to 300 °C and then cooled down to room temperature at a rate of 10 °C/min. For each composition, DSC test was repeated 3 times to ensure the reproducibility of the DSC results.

For reflow, commercial grade polycrystalline copper (Cu) sheets (30 mm × 30 mm × 0.3 mm) were used as substrates. Before soldering, Cu sheets were polished with 2000 Grit silica carbide paper, washed with detergent and soaked in 10 vol.% H_2SO_4 solution for 15–30 min to remove any oxide film present. These were then rinsed with distilled water followed by drying with acetone. Sparkle Flux WF-6317 (Senju Metal Industry, Tokyo, Japan) was then evenly placed on the Cu substrate. SAC-xAl thin disc (diameter = 6.5 mm, thickness = 1.24 mm) were placed in the middle of copper substrates which had been covered with Flux WF-6317. Reflow was carried out in an oven at 250 °C for 60 s. After the reflow process, the residual flux was cleaned and removed by rinsing the sample under running distilled water. After that, the reflowed samples were prepared by standard metallographic specimen preparation for microstructural investigation. The microstructure of the bulk solder and the morphology of the IMCs formed at the solder/substrate interface were investigated by FESEM and the composition of the IMCs was investigated by EDS. IMC thickness was calculated by dividing the IMC area by the length of the IMC using a built-in image analyzer software in an Olympus SZX10 (Olympus, Tokyo, Japan) stereoscope. For each experimental condition, thickness values were measured on 5 micrographs and the average IMC thickness is reported. For the top view observation of the interfacial IMCs, the solders were etched in a mixture of 93% CH_3OH, 5% HNO_3, and 2% HCl to remove the solder matrix and expose the interfacial intermetallic compound.

Vickers hardness measurement was performed to investigate the relationship between microstructure and microhardness. The Vickers hardness values were obtained as [36]:

$$HV = 2P\sin\varphi/2d \quad (2)$$

where φ is the indenter apex angle, P is the applied load and d is the average length of diagonals. The applied load and loading period are 1 kgf and 5 s, respectively. For each specimen, five points were tested and the mean values were obtained.

Nanoindentation testing was done using Hysitron Ubi-750 (Hysitron, Minneapolis, MI, USA). Two modes of indentation were conducted on the samples: Quasi-static and Continuous Dynamic Measurement. Quasi-static indentation was conducted with a maximum load of 500 μN, holding time of 2 s, loading rate and unloading rate of 16.67 μN/s and continuous dynamic measurement test

was conducted with a maximum of 1000 μN, holding time of 2 s and a loading rate and unloading rate of 16.67 μN/s. For each element, 5 points were tested and the mean values were obtained. The load–displacement data obtained were analyzed using the method proposed by Oliver and Pharr [37] to determine the hardness and elastic modulus as functions of the displacement of the indenter. For quasi static nanoindentation testing, hardness (H) and reduced modulus (E) can be obtained. The elastic modulus E of the material being indented is related to the reduced modulus using the following equation [38]:

$$E = \frac{1 - v^2}{\frac{1}{E_r} - \frac{1-v_i^2}{E_i}} \quad (3)$$

where v is the Poisson's ratio of the indented material (usually assumed to be 0.3 if unknown), and v_i and E_i are the Poisson's ratio and elastic modulus of the indenter tip material, respectively. The elastic modulus E_i and Poisson's ratio v_i of the Berkovich indenter used in this study are 1141 GPa and 0.07 respectively. For continuous dynamic measurement, results for the hardness and complex modulus as a function of indentation depth can be obtained.

Complex modulus, which is also known as dynamic modulus, is a ratio of stress strain under vibratory conditions. It could be defined by the equation below [39]:

$$E^* = E' + iE'' \quad (4)$$

where E* is the reduced complex modulus, E′ is the reduced storage modulus (or elastic modulus), E″ is the loss modulus and i is the imaginary unit.

5. Conclusions

The following conclusions can be drawn from this study:

- Minor addition of Al has reduced the undercooling of SAC105 solder significantly.
- With addition of 0.1–0.5 wt.% Al to SAC105, Cu_3Al_2 IMC was found.
- Cu_3Al_2 IMC segregated near the edge of solder upon reflow as Al was added up to 0.3 wt.%.
- Minor alloying Al has reduced the thickness of interfacial Cu_6Sn_5 IMC significantly but do not alter the morphology of Cu_6Sn_5 IMC.
- Minor alloying Al has reduced the thickness of interfacial Cu_6Sn_5 IMC but has no significant effect on the thickness of Cu_3Sn during isothermal aging.
- It is suggested that the influence of Al exert its influence on the interfacial reaction by hindering the flow of reacting species at the interface during reflow.
- Cu_3Al_2 IMC has higher hardness and elastic modulus than other microstructure in SAC105 + Al microstructures.

Acknowledgments: The authors would like to acknowledge the financial support from High Impact Research (HIR) Grant, University of Malaya (Project No. UM.C/625/1/HIR/MOHE/ENG/26).

Author Contributions: Y.M.L. and A.S.M.A.H. conceived and designed the experiments; Y.M.L. performed the experiments; Y.M.L. and A.S.M.A.H. analyzed the data; A.S.M.A.H. contributed reagents/materials/analysis tools; and Y.M.L. and A.S.M.A.H. wrote the paper.

Conflicts of Interest: The authors declare no conflict of interest.

References

1. Kang, S.K.; Shih, D.-Y.; Leonard, D.; Donald, N.Y.; Henderson, D.W.; Gosselin, T.; Sarkhel, A.; Goldsmith, N.Y.C. Ag_3Sn plate formation in the solidification of near-ternary eutectic Sn-Ag-Cu. *JOM* **2004**, *56*, 34–38. [CrossRef]
2. Shnawah, D.A.A.; Sabri, M.F.M.; Badruddin, L.A.; Said, S.B.M.; Che, F.X. The bulk alloy microstructure and mechanical properties of Sn-1Ag-0.5Cu-xAl solders (x = 0, 0.1 and 0.2 wt%). *J. Mater. Sci. Mater. Electron.* **2012**, *23*, 1988–1997. [CrossRef]

3. Burke, C.; Punch, J.A. Comparison of the Creep Behavior of Joint-Scale SAC105 and SAC305 Solder Alloys. In Proceedings of the IEEE Transactions on Components, Packaging and Manufacturing Technology, Kyoto, Japan, 12 February 2014; pp. 516–527.
4. Cheng, F.; Gao, F.; Zhang, J.; Jin, W.; Xiao, X. Tensile properties and wettability of SAC0307 and SAC105 low Ag lead-free solder alloys. *J. Mater. Sci.* **2011**, *46*, 3424–3429. [CrossRef]
5. Liu, W.; Lee, N.C. The effects of additives to SnAgCu alloys on microstructure and drop impact reliability of solder joints. *JOM* **2007**, *56*, 26–31. [CrossRef]
6. Lee, T.; Bieler, T.R.; Kim, C.; Ma, H. *Fundamentals of Lead-Free Solder Interconnect Technology*; Springer: New York, NY, USA, 2015.
7. Ahmad, A.E. Evolution of microstructure, thermal and creep properties of Ni-doped Sn-0.5Ag-0.7Cu low-Ag solder alloys for electronic applications. *Mater. Des.* **2013**, *52*, 663–670.
8. Kim, K.S.; Huh, S.H.; Suganuma, K. Effects of fourth alloying additive on microstructures and tensile properties of Sn-Ag-Cu alloy and joints with Cu. *Microelectron. Reliab.* **2003**, *43*, 259–267. [CrossRef]
9. Anderson, I.E.; Walleser, J.W.; Harringa, J.L.; Laabs, F.; Kracher, A. Nucleation control and thermal aging resistance of near-eutectic Sn-Ag-Cu-X solder joints by alloy design. *J. Electron. Mater.* **2009**, *38*, 2770–2779. [CrossRef]
10. Shi, Y.W.; Tian, J.; Hao, H.; Xia, Z.; Lei, Y.; Guo, F. Effects of small amount addition of rare earth Er on microstructure and property of SnAgCu solder. *J. Alloys Compd.* **2008**, *453*, 180–184. [CrossRef]
11. Laurila, T.; Vuorinen, V.; Paulasto-Kröckel, M. Impurity and alloying effects on interfacial reaction layers in Pb-free soldering. *Mat. Sci. Eng. R* **2010**, *68*, 1–38. [CrossRef]
12. Amagai, M.A. study of nanoparticles in Sn–Ag based lead free solders. *Microelectron. Reliab.* **2008**, *48*, 1–16. [CrossRef]
13. Gain, A.K.; Chan, Y.C. The influence of a small amount of Al and Ni nano-particles on the microstructure, kinetics and hardness of Sn-Ag-Cu solder on OSP-Cu pads. *Intermetallics* **2012**, *29*, 48–55. [CrossRef]
14. Boesenberg, A.J.; Anderson, I.E.; Harringa, J.L. Development of Sn-Ag-Cu-X Solders for Electronic Assembly by Micro-Alloying with Al. *J. Electron. Mater.* **2012**, *41*, 1868–1881. [CrossRef]
15. Xia, Y.H.; Jee, J.K.; Yu, J.; Lee, T.Y. Effect of aluminum concentration on the interfacial reactions of Sn-3.0Ag-xAl solders with copper and ENIG metallizations. *J. Electron. Mater.* **2008**, *37*, 1858–1862. [CrossRef]
16. Li, J.F.; Agyakwa, P.A.; Johnson, C.M. Effect of trace Al on growth rates of intermetallic compound layers between Sn-based solders and Cu substrate. *J. Alloys Compd.* **2012**, *545*, 70–79. [CrossRef]
17. Kantarcıoğlu, A.; Kalay, Y.E. Effects of Al and Fe additions on microstructure and mechanical properties of SnAgCu eutectic lead-free solders. *Mat. Sci. Eng. A* **2014**, *593*, 79–84. [CrossRef]
18. Kotadia, H.R.; Panneerselvam, A.; Mokhtari, O.; Green, M.A.; Mannan, S.H. Massive spalling of Cu-Zn and Cu-Al intermetallic compounds at the interface between solders and Cu substrate during liquid state reaction. *J. Appl. Phys.* **2012**, *111*, 074902–074906. [CrossRef]
19. Mohd, F.M.S.; Dhafer, A.S.; Irfan, A.B.; Suhana, B.M.S. Effects of aging on Sn-1Ag-0.5Cu solder alloys containing 0.1 wt % and 0.5 wt % Al. *J. Alloys Compd.* **2014**, *582*, 437–446.
20. Dhafer, A.S.; Mohd, F.M.S.; Suhana, B.M.S.; Iswadi, J.; Mohammad, H.M.; Mohamed, B.A.B.; Mohamed, H.E. Interfacial reactions between Cu substrate and Sn–1Ag–0.5 Cu solder containing 0.1 wt.% Al by dipping method. *J. Mater. Sci. Mater. Electron.* **2015**, *26*, 8229–8239.
21. Whitehead, A.J.; Page, T.F. Nanoindentation studies of thin film coated systems. *Thin Solid Films* **1992**, *220*, 277–283. [CrossRef]
22. Song, J.-M.; Huang, B.-R.; Liu, C.-Y.; Lai, Y.-S.; Chiu, Y.-T.; Huang, T.-W. Nanomechanical responses of intermetallic phase at the solder joint interface—Crystal orientation and metallurgical effects. *Mater. Sci. Eng. A* **2012**, *534*, 53–59. [CrossRef]
23. Saunders, N.; Miodownik, A.P. The Cu-Sn (Copper-Tin) system. Alloy Phase Diagram Evaluations. *Bull. Alloy Phase Diagr.* **1990**, *11*, 278–287. [CrossRef]
24. Funamizu, Y.; Watanabe, K. Interdiffusion in the Al–Cu system. *Trans. Jpn. Inst. Met.* **1971**, *12*, 147. [CrossRef]
25. Molnár, A.; Kardos, I.; Molnár, I.; Gácsi, Z. Effect of silver content on the properties of lead-free solders. *Mater. Sci. Eng.* **2014**, *39*, 51–58.
26. Chen, H.-T.; Ya, B.-B.; Yang, M.; Ma, X.; Mingyu, L. Effect of grain orientation on mechanical properties and thermomechanical response of Sn-based solder interconnects. *Mater. Charact.* **2013**, *85*, 64–72. [CrossRef]

27. Maleki, M.; Cugnoni, J.; Botsis, J. Microstructure-based modeling of the ageing effect on the deformation behavior of the eutectic micro-constituent in SnAgCu lead-free solder. *Acta Mater.* **2013**, *61*, 103–114. [CrossRef]
28. Marquesa, V.M.F.; Wunderleb, B.; Johnstona, C.; Granta, P.S. Nanomechanical characterization of Sn–Ag–Cu/Cu joints—Part 2: Nanoindentation creep and its relationship with uniaxial creep as a function of temperature. *Acta Mater.* **2013**, *61*, 2460–2470. [CrossRef]
29. Lotfian, S.; Molina-Aldareguia, J.M.; Yazzie, K.E.; Llorca, J.; Chawla, N. Mechanical characterization of lead-free Sn-Ag-Cu solder joints by high-temperature nanoindentation. *J. Electron. Mater.* **2013**, *42*, 1085–1091. [CrossRef]
30. Karakaya, I.; Thompson, W.T. The Ag-Sn (Silver-Tin) system. *Bull. Alloy Phase. Diagr.* **1987**, *8*, 340–347. [CrossRef]
31. Katoh, R.; Munekata, O.; Toyoda, Y. Tombstoning Prevented by the Use of a Twin-Peak Solder Alloy. U.S. Patent 6554180 B1, 29 April 2003.
32. Kubaschewski, O.; Hari Kumar, K.C. Materials Science International Team MSIT®, Ag-Cu-Sn (Silver-Copper-Tin). In *Non-Ferrous Met. Ternary Systems*; Springer: Berlin, Germany, 2007; pp. 47–62.
33. Massalski, T.B. The Al−Cu (Aluminum-Copper) system. *Bull. Alloy Phase Diagr.* **1980**, *1*, 27–33. [CrossRef]
34. Kotadia, H.R.; Mokhtari, O.; Bottrill, O.M.; Clode, M.P.; Green, M.A.; Mannan, S.H. Reactions of Sn-3.5Ag-Based Solders Containing Zn and Al Additions on Cu and Ni(P) Substrates. *J. Electron. Mater.* **2010**, *39*, 2720–2731. [CrossRef]
35. Chauhan, P.S.; Choubey, A.; Zhong, Z.W.; Pecht, M.G. *Copper Wire Bonding*; Springer: New York, NY, USA, 2014.
36. Haseeb, A.S.M.A.; Leong, Y.M.; Arafat, M.M. In-Situ Alloying of Sn-3.5Ag Solder during Reflow through Zn Nanoparticle Addition and Its Effects on Interfacial Intermetallic Layers. *Intermetallics* **2014**, *54*, 86–94. [CrossRef]
37. Oliver, W.C.; Pharr, G.M. Measurement of hardness and elastic modulus by instrumented indentation: Advances in understanding and refinements to methodology. *J. Mater. Res.* **2004**, *19*, 3–20. [CrossRef]
38. Fischer-Cripps, A.C. *Nanoindentation*, 3rd ed.; Springer: New York, NY, USA, 2011; pp. 2–126.
39. Meyers, M.A.; Chawla, K. *Mechanical Behavior of Materials*, 2nd ed.; Cambridge University Press: Cambridge, UK, 2008.